International Journal of Biotechnology Research ISSN: 0974-6293
Vol.11 No.1 january-June 2018

Investigation of the Role of Mesoscale Detachment Rate Expressions in a Macroscale Model of a Porous Medium Biofilm Reactor

Fazal Abbas[1] & Hermann Eberl[1]

Abstract: Starting from the traditional mesoscopic one-dimensional biofilm model we derive a macroscopic model of a simple porous medium biofilm reactor in the convection dominated, laminar regime. The mesoscopic processes included in this model are biofilm growth due to substrate consumption and biomass loss due to cell death and biofilm detachment. The upscaling to the macroscale leads to a stiff quasilinear hyperbolic system of balance laws. In numerical simulations we investigate the role of the mesoscopic detachment description for the macroscopic model. To this end we compare four mesoscopic detachment models that are based on different model assumptions and lead to different mathematical expressions. We find that the particular choice plays only a minor role for macroscopic behavior, both from a quantitative and qualitative aspect. Similarly, we find that the overall reactor performance is rather insensitive with respect to the parameters of the detachment rate expressions.

MSC: 92D25.

Keywords: Biofilm reactor, Detachment, Balance laws, Numerical simulation.

1. Introduction

Bacterial biofilms are microbial depositions on immersed surfaces [18]. If the environmental conditions sustain growth, bacteria adhere to the surface and form microbial communities that are embedded in and protected by a self-produced layer of extracellular polymeric substances. Biofilms are ubiquitous. Depending on the context, they can be seen as harmful, e.g. in a medical or industrial setting, neutral, e.g. in natural systems, or beneficial, e.g. in environmental engineering technologies. An essential feature of biofilms that distinguishes them from planktonic or suspended microbial populations are substrate gradients, i.e. in different locations of a biofilm the bacteria can experience different growth conditions [33].

The last two decades saw a vast amount of research conducted in mathematical modeling of biofilm processes. Biofilm modeling is in the first place concerned with the mathematical description of the processes on the *mesoscale*, i.e. the actual biofilm length scale, from around 50 microns to 500 microns. In contrast to this, one refers by *microscale* to the length scale of the individual biofilm constituents, i.e. the length scale of bacteria cells, around 1 micron. On the other hand, *macroscale* refers to the length scale of a reactor, usually larger than centimeters or even meters.

Traditional biofilm models are one-dimensional models assuming the biofilm to cover the substratum in a homogeneous layer [39, 38]. Although these models do not account for the spatial irregularity of biofilms that can be observed under the microscope, they have been successfully and almost routinely used by engineers to gain a better understanding of population, resource and degradation dynamics in complex biofilm communities [8]. These biofilm models, which are primarily studied computationally, due to their

[1] Dept. Mathematics and Statistics, University of Guelph, Guelph, ON, Canada.

mathematical complexity, usually include terms accounting for biofilm detachment, i.e. the loss of biomass due to shear forces acting on the biofilm. Detachment in these models is primarily understood as a mechanism that balances biomass growth and allows the biofilm to reach an equilibrium. The various detachment rate functions used in the literature are based on different assumptions. In a recent study [2] it was found that the choice of a particular detachment rate function might not only affect the mesoscale biofilm prediction quantitatively, but also qualitatively. More recently, also two- and three-dimensional mesoscale biofilm models have been developed, using a variety of mathematical concepts, from agent based models, to cellular automata to partial differential equation models. Among these models there are those that emphasize a description of biofilms as spatially structured populations, but there are also many that focus on mechanical and material properties of biofilms, e.g. [3, 10, 11, 26, 40]. The latter question is undoubtedly important for questions of mechanical stability of biofilms on the mesoscale, but it is not understood well whether these mechanical aspects also contribute to the performance of biofilms, e.g. in substrate removal.

In this study we want to investigate the question how important the description of mesoscopic detachment processes is for macroscale models of biofilm systems. More specifically, we focus on biofilms growing in the pore spaces of a porous medium. Systems of this kind arise in bioremediation of soils, biobarrier for groundwater protection, and in certain wastewater treatment processes. Many macroscopic model descriptions of such systems can be found in the literature, primarily for bioremediation applications, e.g. [7, 9, 12, 16, 31, 32, 34]. Usually these models are a priori formulated for the macroscale and the connection between the underlying mesoscopic processes and the macroscopic description are not always clear. The biofilm description in these models is usually very simplified, e.g. by assuming a constant biofilm thickness or by neglecting substrate gradients in the biofilm. In contrast, we will derive a macroscale model from a mesocale model, using an upscaling procedure. This will ensure that mesoscopic processes are correctly incorporated in the macroscopic description. Upscaling of biofilm models to macroscale applications is a relatively recent development, e.g. [4, 15]. Some of these studies focus on the correct treatment of the substrate transport equations but make simplifying assumptions about biofilm growth. Others propose a general volume averaging strategy which often leads to models to complex to be entirely closed or accessible for specific applications. The probably most comprehensive upscaling studies for biofilm models so far are [14, 23] which use (different) multi-dimensional mesoscopic biofilm model as starting point. The upscaled models, however, are too complex to be easily accessible. With the model that we derive in this study, we follow a different philosophy and a different purpose. Starting point is the traditional one-dimensional biofilm model, including biomass production, substrate degradation, cell death and biofilm detachment. Goal is to derive a relatively easy to handle conceptual macroscopic biofilm reactor model. In our case this will be a stiff system of two quasilinear hyperbolic balance laws, one for the local biofilm thickness and one for the growth limiting substrate. The model then will be studied numerically using a uniformly accurate centered finite difference scheme that was originally proposed in [19], and is considered very suitable for stiff problems [20]. Our particular focus will be on understanding the role of the mesoscopic detachment process for the macroscopic model. To this end we compare quantitatively simulations of the macroscopic models derived for four different mesoscopic detachment rate functions.

2. Mathematical Model

2.1 System Description and Model Assumptions

We consider a macroscale porous medium reactor of length L_r and width L that consists of many dense, parallel, identical, noncommunicating fissures or fractures. In these channel-like pores bacterial biofilms may form. The pores occupy a void space of fraction p of the entire reactor. We assume that biofilm forms on both boundaries of the pores at the same thickness. Substrate is added to the reactor at the upstream end from where the flow through the reactor is driven by prescribing a constant flow rate Q. We assume that Q is high enough to guarantee convection dominated substrate transport, but still in the laminar regime.

On the mesoscopic level, we consider small, square segments of length $\epsilon \ll \min\{L_r, L\}$, which we refer to as cell. This is also depicted in Fig. 1. Assuming a convection dominated regime, substrate enters a cell from the upstream neighbor cell and flows into the downstream neighbor cell. Within the cell the biofilms on both boundaries of the pore space have thickness λ_ϵ, the pore itself a diameter p_ϵ. Thus, we are interested in the case $2\lambda_\epsilon < p_\epsilon$. Otherwise the pore channel is entirely clogged by biofilm. In the aqueous phase we assume a laminar, fully developed, parallel flow profile. Since the flow rate is prescribed, a thicker biofilm implies a faster local flow field and increased shear forces acting on the biofilm. Within the cell of size ϵ, the substrate is assumed to be completely mixed in the aqueous phase, but substrate gradients in the biofilm, in the direction perpendicular to the substratum are considered. Similarly, we assume the biofilm thickness to be spatially constant within one cell. Both the biofilm thickness and the substrate concentration vary along the reactor length. The biofilm processes considered on the meso-scale are biofilm growth due to substrate consumption, natural cell death, and detachment of biomass. We assume that detached biomass is immediately washed out of the reactor. In our model there will be only one substrate considered that controls the growth of the biofilm. All other required substrates are assumed to be available in abundance in the bulk fluid. Similarly, we assume a single-species biofilm. The model on the mesoscopic length scale that we use is formulated in the context of traditional one-dimensional biofilm models [2, 38, 39]

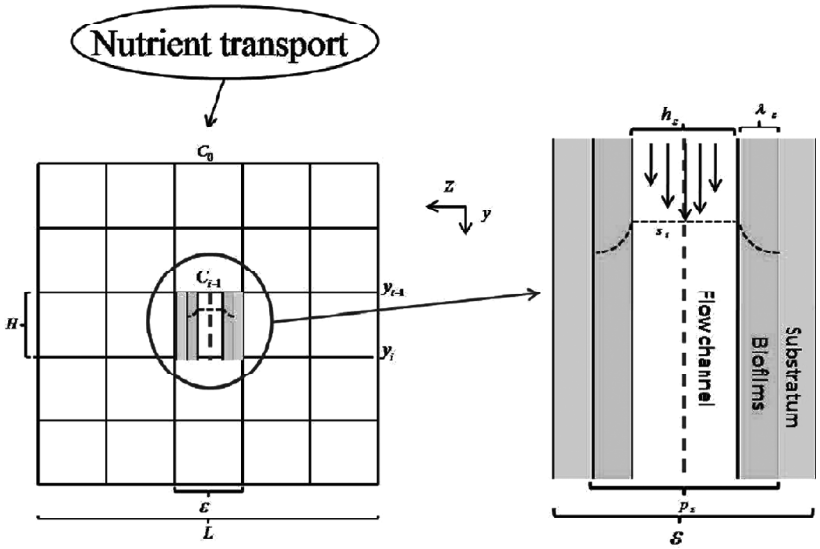

Figure 1: Representation of the macroscopic reactor (left) by mesoscopic cells of size $\epsilon \times \epsilon$ (right). The reactor consists of parallel, non-communicating fissures. The fissures are represented as a sequence of cells of size $\epsilon \times \epsilon$. Each cell contains pore space of size p_ϵ. In each cell biofilm of thickness λ_ϵ grows on both substrata. The flow in each cell is assumed to be Poiseuille flow, i.e. a quadratic flow profile. The flow through the reactor is driven by prescribing a global flow rate Q. The macroscopic model is obtained from a mesoscopic biofilm model by letting $\epsilon \to 0$.

The transition from the mesoscopic to the macroscopic model description is made by passing the size ë of the mesoscopic element to 0.

2.2 Governing Equations

In the ith cell, biofilm net growth is determined by the availability of substrates, such as nutrients or oxygen (in the aerobic case), cell death and biomass loss due to detachment. Following the traditional one-dimensional biofilm modeling, we assume the biofilm to be incompressible, i.e. we assume the biomass density to be constant X_∞ throughout the biofilm. Thus, production of new biomass translates directly into increase of the biofilm thickness $\lambda_{i,\epsilon}$. The velocity with which biomass moves in the biofilm in the i^{th} cell is therefore given by

$$u_i(z,t) = \int_0^{\lambda_{i,\epsilon}} \left(\frac{\mu c_i(z)}{\kappa + c_i(z)} - k_d \right) dz, \qquad 0 < z \le \lambda_{i,\epsilon}$$

where at position z in the biofilm new biomass is produced at rate $\frac{\mu c_i(z)}{\kappa + c(z)}$. Here, μ is the maximum specific growth rate and $c_i(z)$ the concentration of the growth controlling substrate. The constant κ is called the half saturation concentration. By k_d we denote the biomass death rate. The growth controlling substrate diffuses in the biofilm and it is consumed by the bacteria for growth. It is obtained as the solution of the two-point boundary value problem

$$D \frac{d^2 c_i}{dz^2} = \frac{\mu X_\infty}{Y} \frac{c_i}{\kappa + c_i}, \qquad \frac{dc_i}{dz}(0) = 0, \qquad c_i(\lambda_{i,\epsilon}) = C_i, \tag{1}$$

where Y is a yield coefficient for the conversion of substrate into biomass. The convective contribution of the moving biomass to substrate transport is neglected with the usual time scale arguments [38]. The biofilm thickness $\lambda_{i,\epsilon}$ is obtained as the balance of net growth and detachment. Assuming volumetric biofilm detachment, as in [21, 2], we have

$$\frac{d\lambda_{i,\epsilon}}{dt} = u_i(\lambda_{i,\epsilon}) - d(\lambda_{i,\epsilon})\lambda_{i,\epsilon} = \int_0^{\lambda_{i,\epsilon}} \left(\frac{\mu c_i(z)}{\kappa + c_i(z)} - k_d \right) dz - d(\lambda_{i,\epsilon}), \qquad 0 < z \le \lambda_{i,\epsilon}, \tag{2}$$

where the function $d(\lambda)$ is the detachment rate. The substrate concentration in the biofilm in the ith cell depends on the substrate concentration C_i in the aqueous phase via the boundary conditions of (1). It satisfies the mass balance

$$\frac{d(V_i C_i)}{dt} = q_{i-1,\epsilon} C_{i-1} - g_{i,\epsilon} C_i - 2\epsilon J_{i,\epsilon}, \tag{3}$$

where $q_{i,\epsilon}$ is the specific flow rate. V_i is the volume of the aqueous phase, which also depends on the biofilm thickness, i.e.

$$V_i = \epsilon(p_{i,\epsilon} - 2\lambda_{i,\epsilon}), \tag{4}$$

In particular V_i changes as the biofilm grows. The first term on the right hand side of (3) accounts for substrate inflow from the upstream neighboring compartment, at concentration C_{i-1}, and for outflow into the downstream neighboring concentration at concentration C_i. The second term accounts for the substrate flux into the biofilm. It is obtained as

$$J_{i,\epsilon}(C_i, \lambda_{i,\epsilon}) = D \frac{dci}{dz}\Big|_{\lambda_{i,\epsilon}}. \tag{5}$$

Note that by integrating (1) once we obtain with the boundary conditions

$$J_{i,\epsilon}(C_i, \lambda_{i,\epsilon}) = D \frac{dc_i}{dz}\Big|_{\lambda_{i,\epsilon}} = \frac{X_\infty}{Y} \int_0^{\lambda_{i,\epsilon}} \frac{\mu c_i(z)}{\kappa + c_i(z)} dz. \tag{6}$$

Using (4), (5), (6), the mesoscopic equations (2), (3) for the substrate concentration C_i and the the biofilm thickness $\lambda_{i,\epsilon}$ in the ith cell become finally

$$[p_{i,\epsilon} - 2\lambda_{i,\epsilon}] \frac{dC_i}{dt} - 2C_i \frac{d\lambda_{i,\epsilon}}{dt} = \frac{q_{i-1,\epsilon} C_{i-1} - q_{i,\epsilon} C_i}{Y} - 2J_{i,\epsilon}(C_i, \lambda_{i,\epsilon}) \tag{7}$$

and

$$\frac{d\lambda_{i,\epsilon}}{dt} = j_{i,\epsilon}(C_i, \lambda_{i,\epsilon}) - k_d \lambda_{i,\epsilon} - d(\lambda_{i,\epsilon})\lambda_{i,\epsilon}. \tag{8}$$

where we used

$$j_{i,\epsilon}(C_i, \lambda_{i,\epsilon}) := \int_0^{\lambda_{i,\epsilon}} \frac{\mu c_i(z)}{\kappa + c_i(z)}\, dz = \frac{Y}{X_\infty} J_{i,\epsilon}(C_i, \lambda_{i,\epsilon})$$

We normalize the pore space $p_{i,\epsilon}$ and the biofilm thickness $\lambda_{i,\epsilon}$ with respect to ϵ, and rescale the local flow rate $q_{i,\epsilon}$ accordingly. I.e. we introduce the new dimensionless variables

$$p_i = \frac{p_{\epsilon,i}}{\epsilon}, \qquad \lambda_i = \frac{\lambda_{i,\epsilon}}{\epsilon}.$$

Here, p denotes the void fraction of the (empty) porous medium, and 2λ denotes the fraction of the porous medium that is locally occupied by a biofilm.

Substituting this into (8) and (7) leads to

$$\epsilon[p_i - 2\lambda_i]\frac{dC_i}{dt} - 2\epsilon C_i \frac{d\lambda_{i,\epsilon}}{dt} = \frac{q_{i-1,\epsilon}C_{i-1} - q_{i,\epsilon}C_i}{\epsilon} - 2J_{i,\epsilon}(C_i, \epsilon\lambda_i), \tag{9}$$

and

$$\frac{d\lambda_i\epsilon}{dt} = j_{i,\epsilon}(C_i, \lambda_i\epsilon) - k_d\lambda_i\epsilon - d(\lambda_i\epsilon)\lambda_i\epsilon. \tag{10}$$

The transition from the mesoscopic, spatially discrete model (9), (10) for an ϵ-cell to a continuous macroscopic model will be accomplished by passing $\epsilon \to 0$. In preparation of this step we note the following small results.

Lemma 2.1: Let $c(z)$ be the solution of the two-point boundary value problem

$$\frac{d^2c}{dz^2} = A\frac{c}{\kappa + c}, \qquad \frac{dc}{dz}\Big|_{z=0} = 0, \qquad c(\Lambda) = C, \tag{11}$$

with $A > 0$ and $j(C, \Lambda) = D\frac{dc}{dz}(\Lambda)$. Then

$$C\sqrt{\frac{A}{\kappa + C}}\tanh\left(\sqrt{\frac{A}{\kappa + C}}\,\Lambda\right) \le \frac{dc}{dz}(\Lambda) \le A\frac{C}{\kappa + C}\Lambda. \tag{12}$$

Proof: We consider the two auxiliary linear boundary value problems

$$\frac{d^2c_1}{dz^2} = A\frac{c_1}{\kappa + C}, \qquad \frac{dc_1}{dz}\Big|_{z=0} = 0, \qquad c_1(\Lambda) = C,$$

and

$$\frac{d^2c_2}{dz^2} = A\frac{C}{\kappa + C}, \qquad \frac{dc_2}{dz}\Big|_{z=0} = 0, \qquad c_2(\Lambda) = C.$$

Since $c = 0$ is a lower solution for (11) and $c = C$ an upper solution, we have $0 \le c(z) \le C$. Hence, because of

$$A\frac{c}{\kappa + C} \le A\frac{c}{\kappa + c} \le A\frac{C}{\kappa + C}$$

it follows from standard comparison theorems for two-point boundary value problems [6, 37] that

$$c_2(z) \le c(z) \le c_1(z).$$

Moreover, since $c_1(\Lambda) = c(\Lambda) = c_2(\Lambda) = C$ it follows that

$$\frac{dc_2}{dz}(\Lambda) \ge \frac{dc}{dz}(\Lambda) \ge \frac{dc_1}{dz}(Ł).$$

As solutions of linear boundary value problems, the functions $c_1(z)$ and $c_2(z)$ can be obtained as

$$c_1(z) = C\frac{e^{\sqrt{\frac{A}{\kappa + C}}z} + e^{-\sqrt{\frac{A}{\kappa + C}}z}}{e^{\sqrt{\frac{A}{\kappa + C}}\Lambda} + e^{-\sqrt{\frac{A}{\kappa + C}}\Lambda}}$$

and

$$c_2(z) = C + \frac{1}{2}A\frac{C}{\kappa + C}(z^2 - \Lambda^2),$$

whence by differentiation

$$\frac{dc_1}{dz}(\Lambda) = C\sqrt{\frac{A}{\kappa + C}}\tanh\left(\sqrt{\frac{A}{\kappa + C}}\Lambda\right)$$

and

$$\frac{dc_2}{dz}(\Lambda) = \frac{A\Lambda C}{\kappa + C}.$$

Remark 2.2: Expanding the lower estimate $\frac{dc_1}{dz}(\Lambda)$ for $\frac{dc}{dz}$ in the above Lemma in terms of Λ, we find for small enough Λ that

$$\frac{dc_1}{dz}(\Lambda) = C\Lambda\frac{A}{\kappa + C} - \frac{1}{3}\Lambda^3\left(\frac{A}{\kappa + C}\right)^3 + \mathcal{O}(\Lambda^5)$$

i.e. for small enough Λ,

$$\frac{dc}{dz}(\Lambda) \approx \frac{A\Lambda C}{\kappa + C}.$$

This estimate was also derived and verified in a different manner in [1], namely based on a homotopy perturbation method argument.

Lemma 2.3: In (9) and (10) we have $j_{i,\epsilon}(C_i, \lambda_i \epsilon) = \mathcal{O}(\epsilon)$.

Proof: This follows directly from Lemma 2.1 and the previous remark.

Before we are able to derive a macroscopic equation from (9) and (10) we need to take a closer look at the flow rate $q_{i,\epsilon}$ and at the detachment rate $d(\lambda)$. Assuming that the flow rate through the reactor is a given constant, Q, it follows that the flow rate in a single pore is

$$q_{i,\epsilon} = \frac{\epsilon}{L} Q . \tag{13}$$

Several detachment rates have been suggested in the biofilm modeling literature. In [2], it was shown that the choice of detachment rate function can have an affect on persistence of the biofilm and whether or not the biofilm will clog its flow channel on the meso-scale. This was achieved by comparing four types of detachment functions, which we we also compare in this study, with a view on their behavior with respect to upscaling from the meso- to the macroscale. They are given by

$$\begin{cases} d_1(\Lambda) = \delta, \\ d_2(\Lambda) = \delta\Lambda, \\ d_3(\Lambda) = \delta\left(\dfrac{\tau}{\tau_0}\right)^{\nu}, \quad 0 < \nu < 1, \\ d_4(\Lambda) = \delta\tau\Lambda, \end{cases} \tag{14}$$

where by δ we denote a constant detachment rate coefficient. We use the same symbol for each detachment rate model although we point out that both its dimensional unit and its numerical value is different for different $d_{1,\ldots,4}$. However, it is always positive.

In d_1 the detachment rate is constant. This has been used in [25, 28, 35] and other studies. In d_2 the detachment rate grows proportionally with the biofilm thickness. This criterion has become the *de facto* standard detachment criterion. It has been proposed in [36] and used since in numerous studies, such as [5, 38, 39] and many investigations that use existing biofilm modeling software packages. On the mesoscale, both d_1 and d_2 can lead to an asymptotically stable equilibrium, which however, depending on parameters, is not necessarily bounded by the flow channel height [2]. If this is the case the models break down. The stable equilibrium can be trivial (no biofilm) if the substrate supply is too low for a biofilm to form.

The detachment rate d_3 accounts for the experimental observation that the detachment rate depends on the bulk flow hydrodynamics. In this expression τ is the hydrodynamic shear rate acting on the biofilm. It changes as the biofilm grows, i.e. $\tau = \tau(\lambda)$. It also depends on the reactor type and operating conditions. The exponent ν has been derived from experimental data, a default value is $\nu = 0.58$ [27]. By τ_0 we denote the reference shear stress, i.e. the shear stress acting on the channel walls in an empty reactor, $\tau_0 = \tau(0)$. This is a constant for a given reactor type and flow rate. Note that d_3 is written in slightly different form than was used in [2], but both version are equivalent on the mesoscopic scale, only the constant δ is interpreted differently.

Finally, the detachment rate function $d = d_4(\lambda) = \delta\tau\lambda$ was proposed in [2]. It is assumed to depend on both, the biofilm itself and the hydrodynamic shear rate, reflecting that biofilms are stronger in the inner layers than in the outer layers and that well developed thicker biofilms slough off easier than thin biofilms on the mesoscale [13, 29]. Under constant flow rates, the models d_3 and d_4 always lead to an asymptotically stable equilibrium smaller than the flow channel height, i.e complete clogging of the channel is prevented. The equilibrium can be trivial (i.e. no biofilm) if the substrate supply is too small.

Detachment rate functions $d_{3,4}$ require the shear stress at the biofilm/water interface. If the flow is laminar, as can be assumed in porous medium applications, it can be obtained from the elementary solution

of the Navier-Stokes equations for flow between two stationary parallel plates, which can be found in almost all elementary texts in fluid mechanics, e.g. [22]. With (13) it is

$$\tau(\Lambda) = \frac{12\eta q_\epsilon}{\left(\frac{p_\epsilon}{2} - \Lambda\right)^2}. \tag{15}$$

A more detailed derivation is given in [2]. The parameter η in (15) is the dynamic viscosity of the fluid.

Proposition 2.4: We consider (9),(10) with (13), (14), (15).

(a) If the detachment rate is $d = d_1$, the scaling limit $\epsilon \to 0$ of (9), (10) is obtained as

$$\frac{\partial}{\partial t}\begin{pmatrix}(p-2\lambda)C\\ \lambda\end{pmatrix} + \frac{\partial}{\partial x}\begin{pmatrix}\frac{Q}{L}C\\ 0\end{pmatrix} = \begin{pmatrix}-2J(C,\lambda)\\ j(C,\lambda) - k_d\lambda - \delta\lambda\end{pmatrix}. \tag{16}$$

(b) If the detachment rate is $d = d_2$, the scaling limit $\epsilon \to 0$ of (9), (10) is obtained as

$$\frac{\partial}{\partial t}\begin{pmatrix}(p-2\lambda)C\\ \lambda\end{pmatrix} + \frac{\partial}{\partial x}\begin{pmatrix}\frac{Q}{L}C\\ 0\end{pmatrix} = \begin{pmatrix}-2J(C,\lambda)\\ j(C,\lambda) - k_d\lambda\end{pmatrix}. \tag{17}$$

(c) If the detachment rate is $d = d_3$, the scaling limit $\epsilon \to 0$ of (9), (10) is

$$\frac{\partial}{\partial t}\begin{pmatrix}(p-2\lambda)C\\ \lambda\end{pmatrix} + \frac{\partial}{\partial x}\begin{pmatrix}\frac{Q}{L}C\\ 0\end{pmatrix} = \begin{pmatrix}-2J(C,\lambda)\\ j(C,\lambda) - k_d\lambda - \delta\left(\frac{p}{p-2\lambda}\right)^{2\nu}\lambda\end{pmatrix} \tag{18}$$

(d) If the detachment rate is $d = d_4$, the scaling limit $\epsilon \to 0$ of (9), (10) is obtained as

$$\frac{\partial}{\partial t}\begin{pmatrix}(p-2\lambda)C\\ \lambda\end{pmatrix} + \frac{\partial}{\partial x}\begin{pmatrix}\frac{Q}{L}C\\ 0\end{pmatrix} = \begin{pmatrix}-2J(C,\lambda)\\ j(C,\lambda) - k_d\lambda - \delta\frac{12\eta Q\lambda^2}{L\left(\frac{p}{2}-\lambda\right)^2}\end{pmatrix} \tag{19}$$

where $J(C,\lambda) = \frac{\mu X_\infty}{Y} + \frac{C\lambda}{\kappa + C}$ and $j(C,\lambda) = \frac{Y}{X_\infty} J(C,\lambda)$.

Proof: For every ϵ we introduce continuous $C^\epsilon(t, z)$ and $\lambda^\epsilon(t, z)$ that interpolate $C_i(t)$ and $\lambda_i(t)$, i.e. $C^\epsilon(t, i\epsilon) = C_i(z)$ and $\lambda^\epsilon(t, i\epsilon) = \lambda_i(t)$. We pass to the continuous limit by refining $\epsilon \to 0$. We denote the limits of $C^\epsilon(t, z)$ and $\lambda^\epsilon(t, z)$ by $C(t, z)$ and $\lambda(t, z)$ (if they exist). In Lemma 2.1 it was established that $j(C_i, \epsilon\lambda_{i,\epsilon}) = \mathcal{O}(\epsilon)$. More specifically, by Remark 2.2, $j(C_i, \epsilon\lambda_{i,\epsilon}) = \epsilon\frac{\mu X_\infty}{Y}\frac{C}{\kappa + C_i} + \mathcal{O}(\epsilon^3)$ for small ϵ. Similarly, according to (13), q_ϵ is proportional to ϵ. It remains to verify the dependency of the detachment rate functions on ϵ.

(a) For d_1 we have $d(\lambda) = d_1(\lambda) = \delta$, i.e. $\lim_{\epsilon\to 0} d_1(\epsilon\lambda) = \delta$. Taking the limit $\epsilon \to 0$ in (9), (10) gives directly (16).

(b) For d_2 we have $d(\lambda) = d_2(\lambda) = \delta\lambda$, i.e. $\lim_{\epsilon\to 0} d_2(\epsilon\lambda) = 0$. Taking the limit $\epsilon \to 0$ in (9), (10) gives directly (17).

The detachment rate models $d_{3,4}$ depend on the shear rate at the biofilm/water interface. With (15) this is obtained as

$$\tau(\epsilon\lambda) = \frac{12\eta Q}{\epsilon L\left(\frac{p}{2} - \lambda\right)^2}.$$

Using this we find:

(c) For d_3 we have $d(\lambda) = d_3(\lambda) = \delta\,(\frac{\tau}{\tau_0})^{\nu} = \delta\,(\frac{p}{p-2\epsilon\lambda})^{2\nu}$. Thus, taking the limit $\epsilon \to 0$ in (9), (10) gives (18).

(d) For d_4 we have $d(\lambda) = d_4(\lambda) = \delta\tau\lambda = \delta\,\frac{12\eta Q\lambda}{L(\frac{p}{2}-\lambda)^2}$. Taking the limit $\epsilon \to 0$ in (9), (10) gives directly (19).

In the upscaled model (16) and (18) the detachment effects do not depend directly on the flow conditions, although they might depend on them indirectly, since higher flow rates also imply higher substrate availability which counteracts detachment. Using the detachment model $d_2(\lambda)$, which is among the most frequently used mesoscopic models, the detachment effects are negligible on the macro-scale. Only under detachment model d_4 the dependency of the detachment rate on the local hydrodynamic conditions carries over to the macro-scale. Under d_3 and d_4 the upscaled detachment rates attain a singularity as $\lambda \to \frac{p}{2}$. Thus, there is a critical value of λ, which depends on the model parameters, such that $\frac{d\lambda}{dt} \le 0$, i.e. λ will be bounded by this value, if the initial data are bounded by it.

For small $\lambda \ll p/2$ the model with d_3 behaves like the one with d_1, i.e. the detachment losses are a linear function of the biofilm thickness. For larger values $\lambda \to p/2$, on the other hand it behaves qualitatively like the model with d_4, i.e. the detachment rates blows up. On the other hand, for $\lambda \ll p/2$ the model with d_4 behaves like the model with d_2.

More general, the procedure used in Proposition 2.4 converges to a quasilinear hyperbolic equation of type (16)-(19) if the dependency of the underlying detachment rate function is $d = \mathcal{O}(\epsilon^n)$ for $n \ge 1$. If $n > 1$ then the detachment effects become negligible in the macroscopic limit. If on the other hand $n < 1$ the detachment rate blows up, i.e. detachment dominates and no biofilm will be able to establish itself.

After introducing the new dependent variable

$$M := C(p - 2\lambda), \tag{20}$$

the equations (16), (17), (18), (19) can be written in conservative form as

$$\frac{\partial}{\partial t}\begin{pmatrix} M \\ \lambda \end{pmatrix} + \frac{\partial}{\partial x}\begin{pmatrix} \frac{Q}{L}\frac{M}{p-2\lambda} \\ 0 \end{pmatrix} = \begin{pmatrix} -2G(M,\lambda) \\ g(M,\lambda) - k_d\lambda - D(\lambda) \end{pmatrix} \tag{21}$$

where

$$g(M,\lambda) = \frac{\mu M\lambda}{\kappa(p-2\lambda) + M}, \qquad G(M,\lambda) = \frac{X_\infty}{Y}\, g(M,\lambda)$$

and the detachment term $D(\lambda)$ as in (16), (17), (18), (19).

The model (21) needs to be completed by specifying initial and boundary conditions. We consider a reactor of finite length Lr and denote the initial data by

$$c(0,x) = c_0(x), \quad \lambda(0,x) = \lambda_0(x), \quad 0 < x < L_r.$$

We restrict ourselves to treating the case $\lambda_0(x) > 0$ for $0 < x < L_r$. If $\lambda_0(x) = 0$ on an interval $x_1 < x < x_2$ then the solution of (21) on the stripe $(0, T) \times (x_1, x_2)$ is $c(t, x) = c(t, x_1)$, $\lambda(t, x) = 0$.

We assume c_0 to be non-negative.

The boundary condition requirements are determined by the characteristics of (21). Re-writing (21) in the form

$$\begin{pmatrix} M \\ \lambda \end{pmatrix}_t + \begin{pmatrix} \frac{Q}{L}\frac{1}{p-2\lambda} & \frac{Q}{L}\frac{2M}{(p-2\lambda)^2} \\ 0 & 0 \end{pmatrix} \begin{pmatrix} M \\ \lambda \end{pmatrix}_x = \begin{pmatrix} -2G(M,\lambda) \\ g(M,\lambda) - k_d\lambda - D(\lambda) \end{pmatrix}, \tag{22}$$

we find two characteristic families, determined by the eigenvalues of the system matrix. The characteristic speeds are $\chi_1 = 0$ and $\chi_2 = \frac{Q}{L}\frac{1}{p-2\lambda}$. The latter is variable but positive for $0 < \lambda < p/2$. In fact, $\chi_2 > \frac{Q}{Lp}$. For $\lambda > p/2$ the model breaks down. Hence, with one characteristic emanating from the upstream boundary at $x = 0$ into the domain, we require one boundary condition on the upstream boundary. It takes the form

$$c(t, 0) = C_0(t) = \frac{M_0}{p - 2\lambda}.$$

Note that the biofilm thickness at the upstream boundary can be obtained by integrating

$$\frac{d\lambda}{dt} = g(M_0(t), \lambda) - k_d(\lambda) - d(\lambda)\lambda,$$

with

$$M_0(t) = C_0(t)(p - 2\lambda(t)).$$

2.3 Steady State Solution

The hyperbolic system (16)-(19) with the constant boundary condition $C_0(t) = C_0 = const$ permits the trivial steady state solution $(C, \lambda) = (C_0, 0)$. Linearization about this equilibrium shows that it is unstable if $C_0 > \hat{C} := \frac{\kappa(k_d + d(0))}{\mu - k_d - d(0)}$ and stable if $C_0 < \hat{C}$. However, the analysis of the semi-discrete (in space) model, see Appendix A, suggests that a stable non-trivial equilibrium may be found if $C_0 > \hat{C}$.

In a nontrivial equilibrium, i.e. in an equilibrium with $\lambda > 0$, the substrate concentration C and the biofilm thickness λ satisfy

$$\frac{\mu C}{\kappa + C} - k_d - d(\lambda) = 0, \tag{23}$$

because of the requirement $\frac{d\lambda}{dt} \le 0$. If the mesoscopic detachment rate $d(\lambda)$ is chosen as d_1 or d_2, this is solved by a unique C, independent of λ, provided $\frac{mu}{\kappa+1} > k_d + d$ (otherwise no such equilibrium exists).

If the mesoscopic detachment rate is d_3 or d_4, then (23) defines a function $C = \tilde{C}(\lambda)$,

$$\tilde{C} = \frac{\kappa(k_d + d(\lambda))}{\mu - k_d - d(\lambda)}. \tag{24}$$

Substituting this into (18)-(19) and using again that all time derivatives vanish in a steady state, leads to

$$\frac{d\lambda}{dx} = -\frac{2X_\infty L}{YQ\kappa\mu}\frac{\lambda(k_d + d(\lambda))(\mu - k_d - d(\lambda))^2}{d'(\lambda)}, \qquad \lambda^*(0) = \Lambda_0, \tag{25}$$

where Λ_0 is obtained as steady state of the biofilm equation at the boundary, i.e. as solution of (23) for boundary concentration C_0. Equation (25) is valid as long as $\tilde{C}(\lambda(x)) > \hat{C}$. Note that the solution of (25) is a monotonically decreasing function and that $\lambda = 0$ is a special solution of (25). Thus, indeed $\lambda(x) > 0$ for all $x \in (0, L_r)$. Together with (23) this defines a non-homogeneous steady state solution $(C^*(x), \lambda^*(x))$ of (18) or (19).

For most applications, the leading coefficient $\frac{2X_\infty L}{YQ\kappa\mu} \gg 1$. This indicates that the steady state biofilm thickness λ drops quickly, i.e that eventually a relatively thin active layer of biomass is found upstream.

2.4 Non-Steady Solutions Along Characteristics

In Section 2.2 the characteristic speeds were obtained from (22) as $\chi_1 = 0$ and $\chi_2 = \frac{Q}{L}\frac{1}{p-2\lambda}$. The corresponding left-eigenvectors are

$$e_1 = (0, 1)^T$$

and

$$e_2 = \left(1, \frac{2M}{p-2\lambda}\right)^T = (1, 2C)^T.$$

Hence, following [41], (21) in characteristic form is obtained as

$$\frac{d\lambda}{dt} = j(c, \lambda) - k_d\lambda - D(\lambda)\lambda \quad \text{along the lines} \quad \frac{dX_1}{dt} = 0 \tag{26}$$

and

$$\frac{dC}{dt} = -2\frac{\mu\left(\frac{X_\infty}{Y} - C\right) j(C, \lambda) - C(k_d + D(\lambda))\lambda}{p-2\lambda} \quad \text{on} \quad \frac{dX_2}{dt} = \frac{Q}{L}\frac{1}{p-2\lambda}. \tag{27}$$

The last equation implies that along the characteristic curve $X_2(t)$ the substrate concentration decreases, provided $0 < c_0(X_2(0)) < \frac{X_\infty}{Y}$ for characteristics that emanate from the initial data, or $0 < C_0 < \frac{X_\infty}{Y}$ for characteristics that start at the boundary. For realistic parameters, this is not a severe restriction. Moreover, since $\chi_2 > 0$, the characteristic $X_2(t)$ moves downstream as t increases. Thus, it follows that the substrate concentration will decrease both in x and t. The rate of decrease is dominated by $\frac{X_\infty}{Y}\lambda$, which can be very large provided λ is not too small. This indicates that a rapid depletion can be expected in areas with considerable biofilm present.

3. NUMERICAL SIMULATION

3.1 Numerical Method

The development of numerical integration schemes for quasilinear hyperbolic systems has been an active area of research for many years.

The focus of this development has been primarily on conservation laws, i.e. transport equations without reaction terms. Many of these methods cannot be applied directly to balance laws with non-linear reaction terms of the form

$$u_t + (f(u))x = h(u).$$

In our case (20), we have for the dependent variable, the flux and the relaxation term

$$u = \begin{pmatrix} M \\ \lambda \end{pmatrix}, \qquad f(u) = \begin{pmatrix} \dfrac{QM}{L(p-2\lambda)} \\ 0 \end{pmatrix}$$

and

$$h(u) = \begin{pmatrix} -2G(M,\lambda) \\ g(M,\lambda) - k_d\lambda - D(\lambda)(\lambda) \end{pmatrix}.$$

Due to the disparity in time scales of biofilm growth and substrate depletion, expressed by the factor $\frac{X_\infty}{Y} \gg 1$, the balance law (20) is stiff, which poses additional challenges for the numerical solution. We use a central difference scheme proposed in [19]. It is referred to as *Uniformly accurate Central Scheme of order 2* (UCS2) in [30]. It is *L*-stable and well suited for stiff problems [30]. The method splits reaction and transport terms. The reaction terms are treated implicitly to address questions of stiffness, the transport terms explicitly. The scheme uses two predictor steps for the reaction for intermediate time steps $\Delta t/2$ and $\Delta t/3$, namely

$$u_j^{n+1/2} = u_j^n - \frac{1}{2}\frac{\Delta t}{\Delta x} f_j' + \frac{\Delta t}{2} h(u_j^{n+1/2})$$

$$u_j^{n+1/3} = u_j^n - \frac{1}{3}\frac{\Delta t}{\Delta x} f_j' + \frac{\Delta t}{3} h(u_j^{n+1/3})$$

where the upper index n denotes the time step and the lower index *j* the grid position, and f_j' is a suitable finite difference approximation of the derivative of the flux. The simplest one proposed in [19] is

$$f_j' = MM(f_{j+1} - f_j, f_j - f_{j-1})$$

where *MM* denotes the min-mod function

$$MM(x,y) = \begin{cases} \operatorname{sgn}(x)\min(|x|,|y|) & \text{if} \quad \operatorname{sgn}(x) = \operatorname{sgn}(y) \\ 0 & \text{otherwise} \end{cases}.$$

This uses only the values at neighboring grid points. The above predictor steps are used to compute solution at the new time level, at staggered grid points, as

$$u_{j+1/2}^{n+1} = \frac{1}{2}(u_j^n + u_{j+1}^n) + \frac{1}{8}(u_j' - u_{j+1}') - \frac{\Delta t}{\Delta x}(f(u_{j+1}^{n+1/2}) - f(u_j^{n+1/2})) + \Delta t\left(\frac{3}{8}h(u_j^{n+1/3}) + \frac{3}{8}h(u_{j+1}^{n+1/3} + \frac{1}{4}h(u_{j+1/2}^{n+1}))\right).$$

Thus, the method is grid-point explicit but locally implicit in the sense that for the calculation of the new values in a grid point only already computed values from other grid points are required, but to determine the new values *v* in the present grid point three non-linear systems of the type $v = \tilde{v} + \tau h(v)$ must be solved. This can be carried out with general purpose nonlinear equation solvers like Newton's method or fix point iterations, or one can tailor a method specific to the form of the relaxation term $h(v)$. We use the former approach.

3.2 A Typical Simulation

To illustrate the model behavior we show the results of two typical numerical simulations. In one, the substrate C is a major growth controlling nutrient, such as carbon. In the second simulation, while the substrate is still necessary for growth, it is required in smaller amounts. For better comparability of results we use the same reaction parameters in both cases, with the exception of the yield coefficient that expresses how much biomass is produced per unit mass of substrate. In the first case, we choose the yield coefficient from the literature [38], for the second scenario we increase the yield coefficient by a factor 10. The flow rate Q is chosen in a range corresponding to a Peclet number clearly greater than one, i.e. in the convection dominated regime, but a Reynolds number well below 103, i.e. in the laminar regime. The parameters used in the simulations are summarized in Table 3.2.

Table 1
Model Parameter Values Used in the Simulations

Parameter	*Symbol*	*Value*	*Unit*	*Reference*
substrate inflow concentration	C_o	30	gm^{-3}	[38]
biomass density	X_∞	10000	gm^{-3}	[38]
maximum growth rate	μ	6	d^{-1}	[38]
half saturation concentration	κ	4	gm^{-3}	[38]
cell death rate	k	0.4	d^{-1}	[38]
yield coefficient	Y	varied	–	assumed
detachment rate	d	varied	–	assumed
detachment coefficient	ν	0.58	–	[27]
bulk viscosity	η	86.6	Ndm^{-2}	[17]
bulk density	ρ	1 ¡£ 10^6	gm^{-3}	[17]
flow rate	Q	0.5	m^2d-1	assumed
reactor width	L	0.1	m	assumed
reactor length	L_3	0.3	m	assumed

For initial data we assume a small background concentration of substrate, at the level of the half saturation concentration,

$$c_0(x) = \kappa, \qquad 0 < x \le L$$

and a non-homogeneous biomass distribution at low level. More specifically, we assume that more biomass is initially found in the center of the reactor, parameterized by

$$\lambda_0(x) = 0.001 e^{-10(\frac{x}{L_r}-12)^2}.$$

At the inflow boundary, the substrate concentration is kept constant at

$$C_0 = 7.5\,\kappa,$$

i.e. clearly above the half saturation concentration, but low enough that substrate is not considered abundant. More specifically, we have $C_0/(\kappa + C_0) \approx 0.88 < 1$.

For this first simulation, we use the constant detachment rate model, as in (16). We choose $\delta = 0.5d^{-1}$, i.e. the combined biomass loss rate, cell death and detachment, is not negligible compared to the maximum specific growth rate.

We first discuss the first scenario, with yield coefficient $Y = 0.63$. When the simulations starts, the bacteria along the reactor immediately start the degradation of the available substrate. The substrate plume moves in from the upstream boundary. About halfway through the channel, where the initial biomass

concentration is highest, it is almost completely depleted. An extended, almost depleted zone which reaches from the downstream end upstream develops. In this depleted zone living conditions for the bacteria are less favorable than at the upstream end where fresh medium is supplied and substrate is available at higher concentrations. This leads to an accelerated growth of biomass upstream and what appears to be an upstream movement of bacteria. However, since in our model the bacteria are stationary this is in fact a reaction wave propagating toward the inflow boundary. Eventually, the active biomass accumulates upstream in a narrow region, whereas further downstream no substrate is available for notable biomass expansion. This is illustrated in Figures 2(a), (b).

In the case of the yield coefficient $Y = 6.3$, the behavior is qualitatively the same but the substrate depletion is slower and the biomass density grows to substantially higher values. See Figure 2(c), (d). While also here an upstream moving reaction wave with increasing biomass is observed, it is slower. Similarly, while in the previous case substrate on outflow was diminished almost immediately, we note here that the outflow concentration decreases steadily and that complete depletion is observed only after some time.

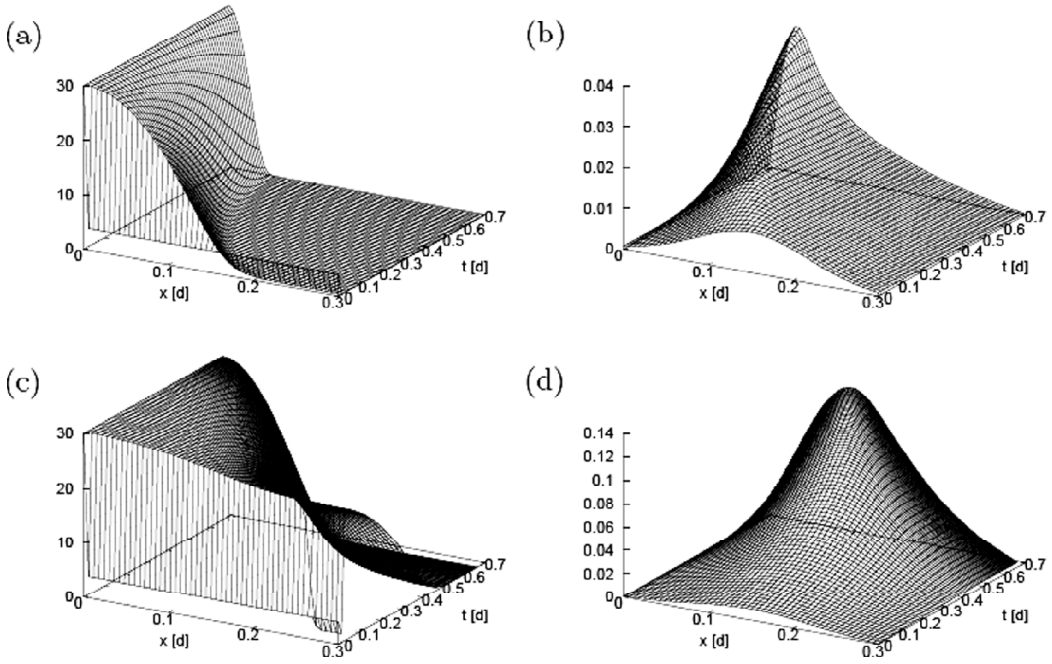

Figure 2: Simulation of model (16) with the parameters in Table 3.2 and the initial and boundary conditions as described in Section 3.2. The top row shows the case of low yield coefficient $Y = 0.63$: (a) substrate concentration, (b) relative biofilm thickness. The bottom row shows the case of high yield coefficient $Y = 6.3$: (c) substrate concentration, (d) relative biofilm thickness.

3.3 The Influence of the Choice of Detachment Functions

A primary goal of this study is to investigate the effect of the specific form of the detachment rate function on the overall substrate degradation. A quantitative comparison is difficult, because the detachment functions (14) all are based on different processes and factors and involve different model parameters. Therefore, such a comparison is to be taken in qualitative rather than a quantitative sense. To allow for an interpretative comparison we use the detachment rate functions in the following form:

$$d_1(\lambda) = \delta, \qquad d_2 = 0, \qquad d_3(\lambda) = \delta\left(\frac{p}{p-2\lambda}\right)^{\nu}, \qquad d_4(\lambda) = \delta\,\frac{p\lambda}{\frac{p}{2}-\lambda}.$$

Thus, for $\lambda = 0$, d_1 and d_3 take the same value, but $d_3 > d_1$ for $\lambda > 0$. On the other hand, $d_4(0) = 0$ (similar as $d_2 = 0$), but it increases as λ increases. As discussed above, the leading constant in d_4 actually depends on the flow rate and the viscosity of the aqueous phase. However, since we keep those constant we can also choose δ as a constant. The detachment rate functions are plotted in Fig. 3.

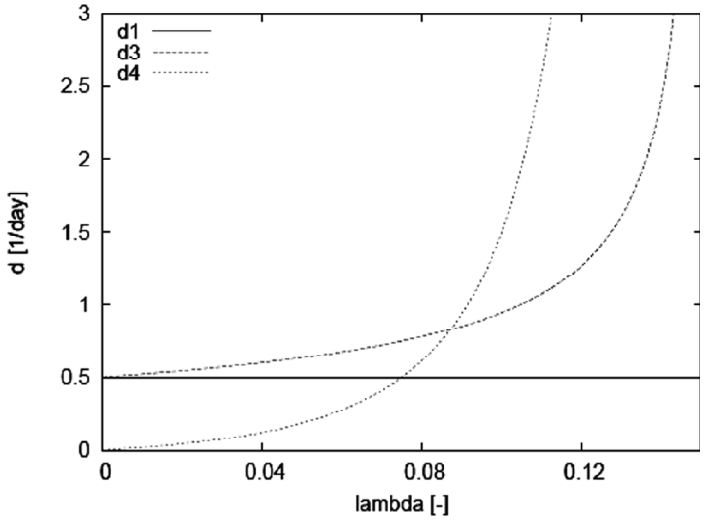

Figure 3: Upscaled detachment rate functions used in this study.

We plot in Fig. 4 the biomass detached from the system for the different detachment rate functions, both for high and default yield coefficient Y. For $Y = 0.63$, the amount of biomass detached is largest for d_3 and smallest for d_4. In all cases it increases with time. In the case of d_1 and d_3, it appears to level off by the end of the simulation time window. For d_2 the amount of biomass detached is initially much lower than for the other two criteria. However, the growing biofilm accelerates detachment, and the difference to the other two criteria becomes smaller. A similar picture is obtained for $Y = 6.3$.

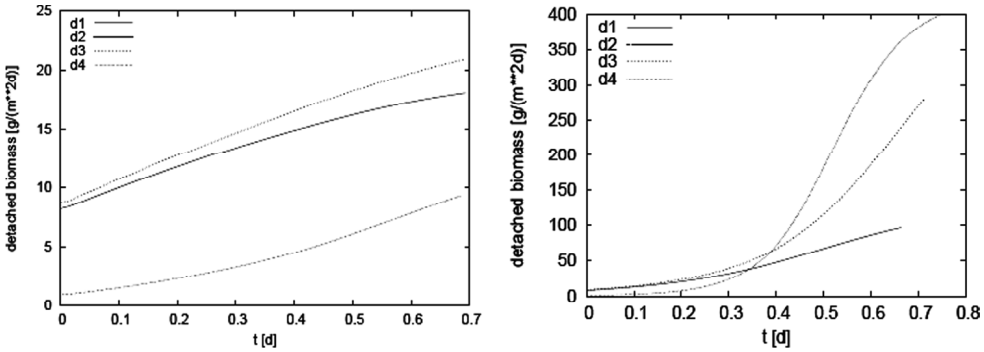

Figure 4: Biomass detached for various detachment rate functions. Left panel: $y = 0.63$. Right panel: $Y = 6.3$.

Initially, as long as the biofilm is small, d_1 and d_3 agree well with each other, while d4 stays clearly below. As the amount of biomass in the system increases, detachment according to d_3 is stronger than in the case of d_1. The biomass detached according to d_4 eventually surpasses both, d_1 and d_3. Overall, the amount of biomass detached is much higher for the higher yield coefficient than for the lower one. This reflects that in the latter case less substrate is required and degraded to produce biomass, i.e. more biomass is being produced. In both cases $Y = 0.63$ and $Y = 6.3$ we observe a clear difference in simulation results w.r.t macroscopic detachment for different mesoscopic detachment rate functions. The criteria d_3 and d_4, which have a singularity for $\lambda = p/2$ show qualitatively a different behavior than the model with constant detachment rate function d_1. They predict higher biomass loss from detachment eventually.

In Fig. 5 we plot the amount of substrate removed from the system as a function of time, i.e. $\frac{Q}{L}(C_0 - c(t, L_r))$, for $Y = 0.63$. The choice of a mesoscopic detachment rate function does not greatly affect the overall reactor performance. The same simulations conducted for the lower yield case $Y = 0.63$ showed no effect of the detachment rate function on susbtrate removal (data not shown). In all four cases, the substrate was swiftly completely degraded.

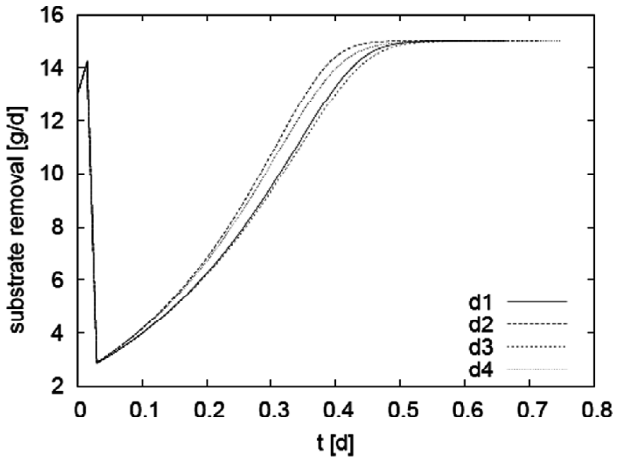

Figure 5: Substrate removed using various detachment rate functions. These simulations were carried out for $Y = 6.3$. A similar simulation for $Y = 0.63$ showed that the detachment rate function has no effect (data not shown).

3.4 Effect of Model Parameters for d_4

In further simulation experiments we focus on the detachment rate function d_4, in which the detachment rate is dynamically adjusted, not only in respect to changes in biofilm thickness but also in response to changing local hydrodynamic conditions at the biofilm/water interfaces. We investigate the sensitivity of the model with respect to the detachment rate function parameters. In one experiment we varied δ over almost one order of magnitude, from $0.1\,p$ to $0.9\,p$. In a second one the flow rate Q is varied from 0.1 to 0.9. Since in the case of the low yield coefficient substrate depletion is almost immediate, we conducted this simulation study for $Y = 6.3$.

In Fig. 6 we plot the model solution λ and c for selected values of δ at fixed $Q = 0.5$. We first note that the simulation results look qualitatively rather similar. The maximum relative biofilm thickness reached decreases by about 25% as the detachment rate coefficient increases by 80%. However, in all cases we observe after about $t = 0.5$ that the substrate is almost depleted. The amount of biomass detached as well as a the amount of substrate degraded are plotted in Fig. 7. In both cases, the qualitative and quantitative differences between the simulations are small. The choice of the detachment rate coefficient does not have notable effect on the substrate removal efficiency in the reactor, and introduces primarily a small time shift in the detachment curves. Thus, these plots confirm that the mesoscopic detachment rate coefficient only plays a minor role on the macroscopic scale.

In a final simulation experiment we vary the reactor flow rate Q from 0.1 to 0.9. Since in detachment rate function d_4 the detachment coefficient scales proportionally with the flow rate, the detachment coefficients are actually the same as in the previous experiment, but changes in the flow rate also affect substrate supply. We plot again for selected values of the varied parameter the relative biofilm thickness and the substrate concentration, see Fig. 8. For the slowest flow rate $Q = 0.1$, substrate is almost completely depleted in the upstream part of the reactor immediately. Biofilm accumulates in the entrance region of the reactor. For faster flow rates, the substrate initially reaches the downstream end but is depleted after a while when the biofilm has the opportunity to establish itself. The higher the flow rate, the longer does it take until depletion is completed. Since substrate is not depleted entirely, a considerable amount of biofilm is

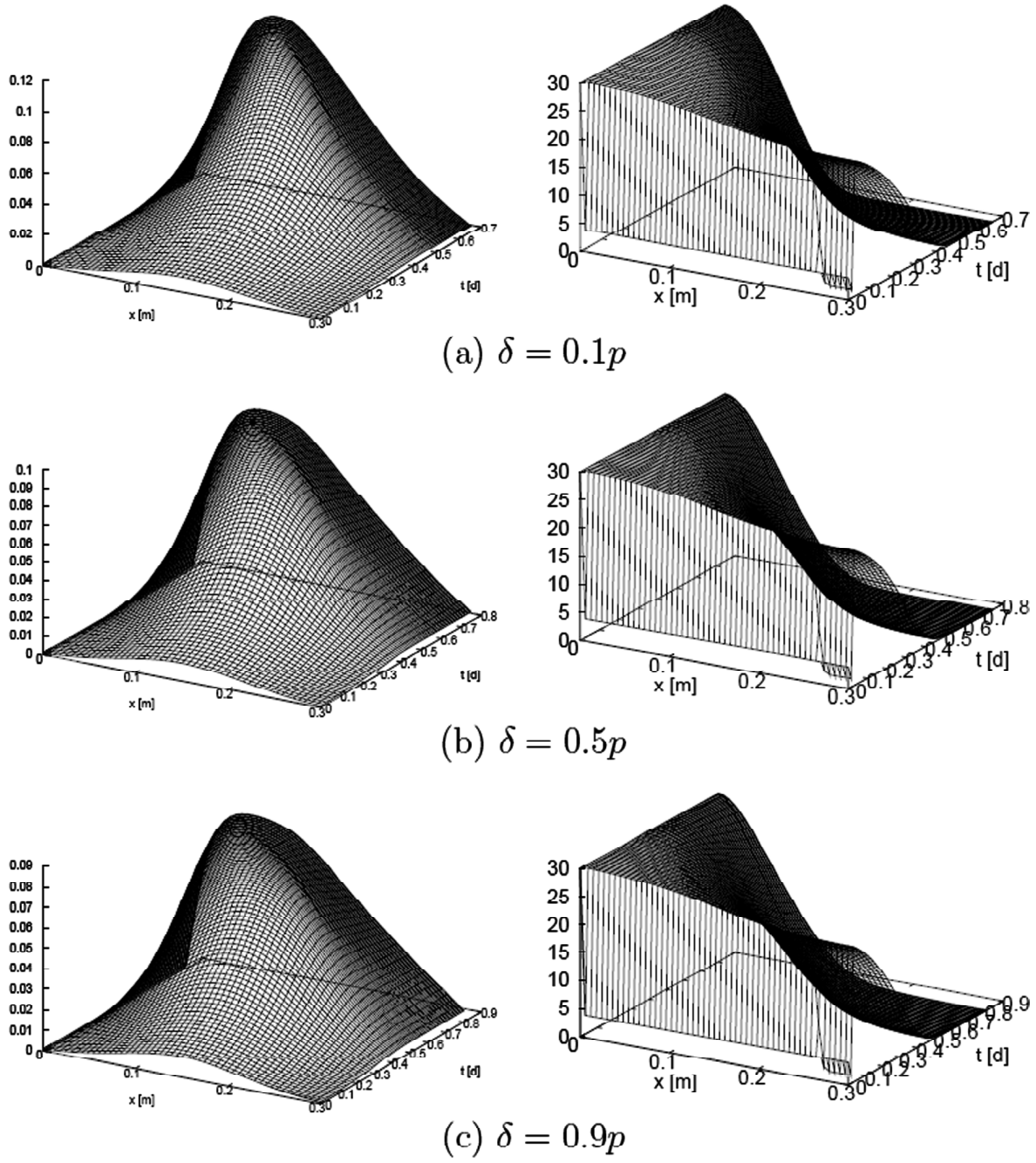

Figure 6: Biofilm thickness λ (left column) and substrate concentration *c* (right column) for selected detachment rate parameters in $d_4(\lambda)$. These simulations were carried out for the high yield coefficient case *Y* = 6.3.

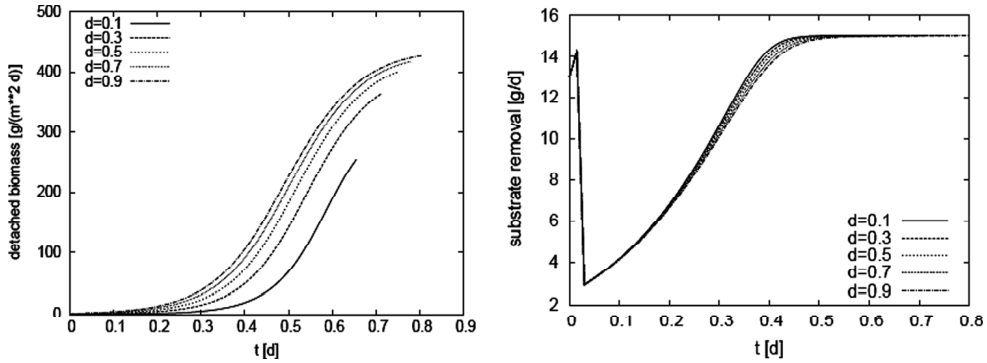

Figure 7: Biomass detached (left) and substrate removed (right) for various detachment rate coefficients δ.

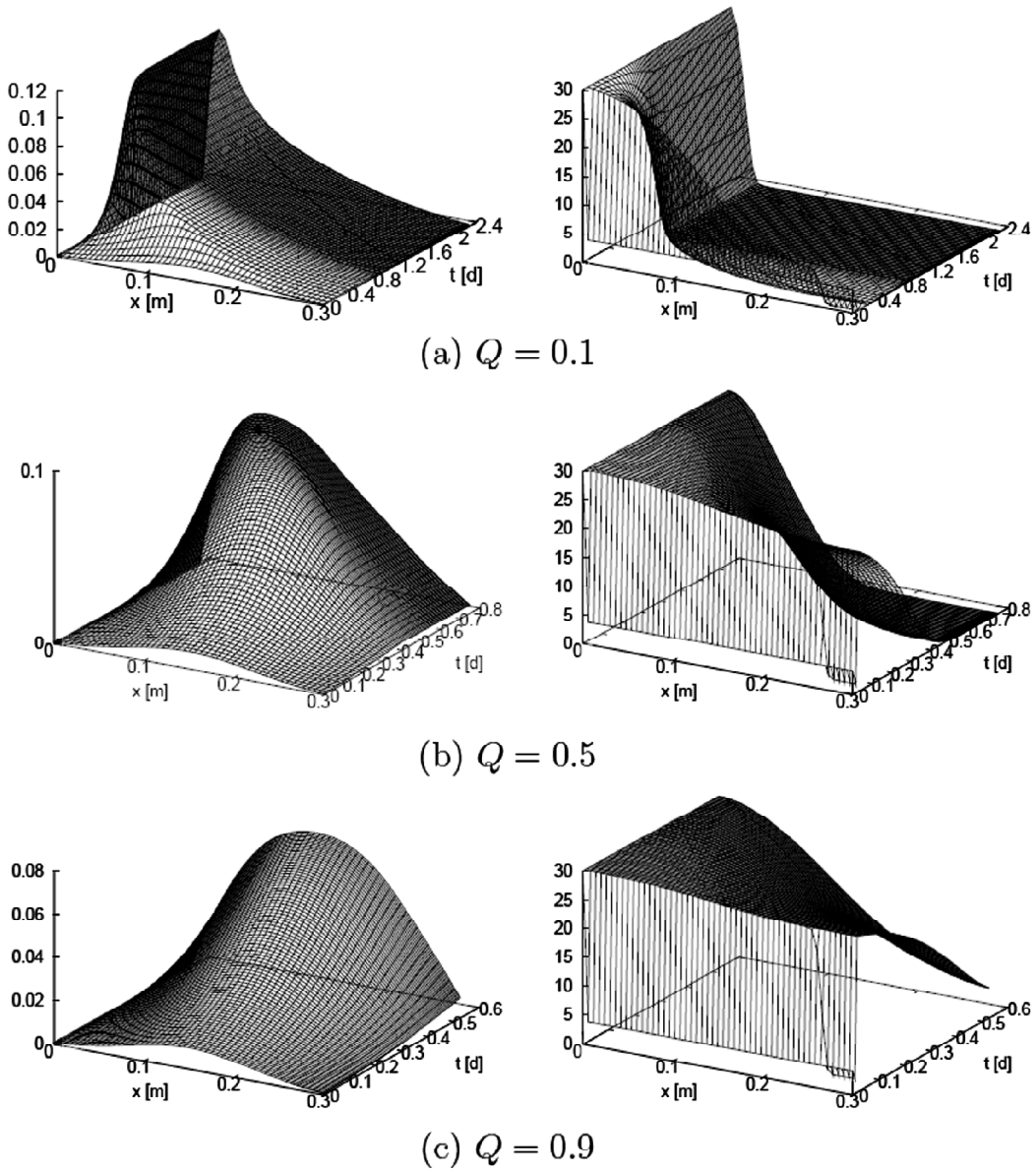

Figure 8: Biofilm thickness λ (left column) and substrate concentration *c* (right column) for selected flow rates *Q*. These simulations were carried out for the high yield coefficient case *Y* = 6.3 with model (19).

found along the reactor. The effect of the flow rate on the maximum biofilm thickness in the reactor is not huge. We note that due to the higher shear forces for faster flows the detachment rate is higher and thus the maximum biofilm thickness smaller. However, the variation in maximum biofilm thickness is smaller than the variation in the flow field applied in this experiment.

In Fig. 9 we plot the substrate removal rate and the amount of biofilm detached from the system as functions of time. At higher reactor flow rates, substantially more biomass is removed from the system than at lower flow rates. This is owed to the increased substrate supply that leads to an increased production of new biomass. Similarly, at higher flow rates the substrate removal efficiency increases. Since eventually substrate is more or less completely depleted, this is entirely due to the increased substrate supply. The faster the flow, the later the system reaches complete depletion.

We note that the differences in the simulations presented here are much bigger than in Fig. 6. This suggests, that changes in the flow, rate, and hence in substrate supply have a much bigger impact on the overall simulation outcome than changes in the detachment coefficient alone.

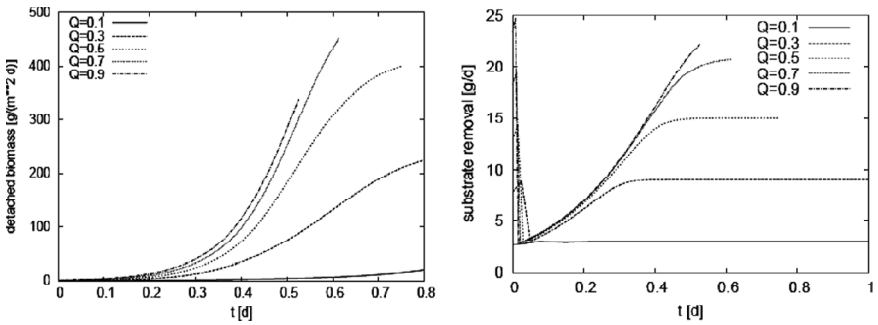

Figure 9: Biomass detached (left) and substrate removed (right) for various flow rates *Q*. These simulations were carried out for the high yield coefficient case Y = 6.3 with model (19).

4. CONCLUSION

In mesoscale models of biofilms, the particular choice of a detachment rate function can greatly affect the long term behavior of the model solution, not only quantitatively but also qualitatively [2].

Using a simple macroscale model that was derived by upscaling the traditional one-dimensional biofilm model for porous medium applications in convection dominated, laminar regimes we find that on the reactor scale, on the other hand, the choice of a detachment rate function plays a much smaller role. Detachment models that are based on very different model assumptions can lead to very similar results.

While the parameters of the detachment model affect the detachment process itself, they do not greatly affect overall system behavior, such as substrate removal efficiency.

Moreover, in the case of detachment models that depend on the reactor flow rate, we find, that the effect of hydrodynamic on detachment is small compared to its effect on substrate transport and availability.

The overall conclusion of our study is that the specific choice of detachment rate expressions, which can play a major role for mesoscopic biofilm simulation studies, are only of minor importance in macroscale simulation studies that focus on substrate removal. This adds justification to the assumption that the detachment process can be neglected in bioremediation and models, such as [12, 34].

REFERENCES

[1] Abbas F., Eberl H. J., (2011), Analytical Substrate Flux Approximation for the Monod Boundary Value Problem, *Appl. Math. Comp.*, **218**(4), 1484-1494.

[2] Abbas F., Sudarsan R., and Eberl H. J., Longtime Behavior of Onedimensional Biofilm Models with Shear Stress Dependent Detachment Rate Functions, *Math. Biosci. Eng.*, (Accepted).

[3] Alpkvist E., and Klapper I., (2007), Description of Mechanical Response Including Detachment Using a Novel Particle Model of Biofilm/Flow Interaction, *Wat. Sci. Tech.*, **55**(8-9), 265-273.

[4] Aspa Y., Debenest G., and Quintard M., (2007), Effect Transport Properties of Porous Biofilms, Eurotherm *Seminar No 81: Reactive Heat Transfer in Porous Media, Ecole des Mines d'Albi*, 8pp.

[5] Bryers J. D., (1984), Biofilm Formation and Chemostat Dynamics: Pure and Mixed Culture Considerations, Biotech. Bioeng., **26**(8), 948-958.

[6] Carl S., and Heikkilä S., (2000), *Nonlinear Differential Equations in Ordered Spaces*, Chapman & Hall.

[7] Chapwanya M., O'Brien S., and Williams J. F., (2010), A Perturbation Solution for Bacterial Growth and Bioremediation in a Porous Medium with Bio-Clogging, *J. Comp. Appl. Math.*, **234**(9), 2709-2723.

[8] Chaudhry M. A. S., and Beg S. A., (1998), A Review on the Mathematical Modeling of Biofilm Processes: *Advances in Fundamentals of Biofilm Modeling, Chem. Eng. & Technol.*, **21**(9), 701-710.

[9] Chen-Carpentier B. M., and Kojouharov H. V., (2003), Numerical Simulation of Dual-Species Biofilm in Porous Media, *Appl. Num. Math.*, **47**, 377-389.

[10] Cogan N. G., (2008), Two-Fluid Model of Biofilm Disinfection, *Bull. Math. Biol.*, **70**(3), 800-819.

[11] Cogan N. G., (2010), An Extension of the Boundary Integral Method Applied to Periodic Disinfection of a Dynamic Biofilm, *SIAM J. Appl. Math.*, **70**, 2281-2307.

[12] Demaret L., Eberl H. J., Efendiev M. A., and Maloszewski P., (2009), A Simple Bioclogging Model that Accounts for Spatial Spreading of Bacteria, *Electr. J. Diff Eqs. CS*, **17**, 51-69.

[13] Derlon N., Massé A., Escudié R., Bernet N., and Paul E., (2008), Stratification in the Cohesion of Biofilms Grown Under Various Environmental Conditions, *Water Research*, **42**(8-9), 2102-2110.

[14] Eberhard J. P., Ewing R. E., and Cunningham A., (2005), Coupled Cellular Models for Biofilm Growth and Hydrodynamic Flow in a Pipe, *Int. J. Multiscale Comp. Eng.*, **3**(4), 499-516.

[15] Golfier F., Wood B. D., Orgogozo L., and Quintard M., (2009), Bues M Biofilms in Porous Media: Development of Macroscopic Transport Equations via Volume Averaging with Closure for Local Mass Equilibrium Conditions, *Adv, Wat. Res.*, **32**(3), 463-485.

[16] Ham Y. J., Kim S. B., and Park S. J., (2007), Numerical Experiments for Bioclogging in Porous Media, *Env. Technology*, **28**, 1079-1089.

[17] Kuchling H., (1987), *Physik*, (18th Ed.), VEB Fachbuchverlag Leipzig.

[18] Lewandowski Z., and Beyenal H., (2007), *Fundamentals of Biofilm Research*, CRC Press.

[19] Liotta S. F., Romano V., and Russo G., (2000), Central Schemes for Balance Laws of Relaxation Type, *SIAM J. Num. An.*, **38**(4), 1337-1356.

[20] Meister A., and Struckmeier J., (Eds), (2002), Hyperbolic Differential Equations, *Theory, Numerics and Applications*, Vieweg.

[21] Morgenroth E., (2003), Detachment: An Often-Overlooked Phenomenon in Biofilm Research and Modelling, In: S. Wuertz, *et al*., (Eds), *Biofilms in Wastewater Treatment*, 246-290, IWA Publishing, London.

[22] Munson B. R., Young D. F., and Okiishi T. H., (1990), *Fundamentals of Fluid Mechanics*, John Wiley & Sons.

[23] van Noorden T. L., Pop I. S., Ebigbo A., and Helmig R., (2010), An Upscaled Model for Biofilm Growth in a Thin Strip, *Wat. Res. Res.*, **46**.

[24] Paramonova E., Kalmykowa O. J., Van Der Mei H. C., Busscher H. J., and Sharma P. K., (2009), Impact of Hydrodynamics on Oral Biofilm Strength, *J. Dent. Res.*, **88**(10), 922.

[25] Peyton B. M., and Characklis W. G., (1982), A Statistical Analysis of the Effect of Substrate Utilization and Shear Stress on the Kinetics of Biofilm Detachment, *Biotech. Bioeng.*, **41**(7), 728-735.

[26] Picioreanu C., van Loosdrecht M. C. M., and Heijnen J. J., (2001), Two-Dimensional Model of Biofilm Detachment Caused by Internal Stress from Liquid Flow, *Biotech. Bioeng.*, **72**(2), 205-218.

[27] Rittmann B. E., (1982), The Effect of Shear Stress on Biofilm Loss Rate, *Biotech. Bioeng.*, **24**, 501-506.

[28] Rittmann B. E., Stilwell D., and Ohashi A., (2002), The Transient-State, Multiple-Species Biofilm Model for Biofiltration Processes, *Water Research*, **36**(9), 2342-2356.

[29] Rochex A., Massé A., Escudié R., Godon J. J., and Bernet N., (2009), Influence of Abrasion on Biofilm Detachment: Evidence for Stratification of the Biofilm, *J. Ind. Microbiol. Biotech.*, **36**(3), 467-470.

[30] Russo G., (2002), Central Schemes and Systems of Balance Laws, In [20], 57-114.

[31] Schäfer D., Schäfer W., and Kinzelbach W., (1998), Simulation of Reactive Processes Related to Biodegradation in Aquifers: 1. Structure of the Three-Dimensional Reactive Transport Model, *J. Cont. Hydr.*, **31**, 167-186.

[32] Seki K, and Miyazaki T., (2001), A Mathematical Model for Biological Clogging of Uniform Porous Media, *Wat. Res. Res.*, **37**(12), 2995-2999.

[33] Stewart P. S., (2003), Diffusion in Biofilms, *J. Bacteriol.*, **185**, 1485-1491.

[34] Thullner M., Schroth M. H., Zeyer J., and Kinzelbach W., (2004), Modeling of a Microbial Growth Experiment with Bioclogging in a Twodimensional Saturated Porous Media Flow Field, *J. Cont. Hydr.* **70**, 37-62.

[35] Tijhuis L., van Loosdrecht MCM, and Heijnen J. J., (1995), Dynamics of Biofilm Detachment in Biofilm Airlift Suspension Reactors, *Biotech. Bioeng.*, **45**(6), 481-487.

[36] Trulear M. G., and Characklis W. G., (1982), Dynamics of Biofilm Processes, *J. Water Pollut. Control Fed.*, **54**(9), 1288-1301.

[37] Walter W., (2000), *Gewöhnliche Differentialgleichungen*, Springer, (7th Ed.).

[38] Wanner O., Eberl H. J., Morgenroth E., Noguera D. R., Picioreanu C., Rittmann B. E., and van Loosdrecht M. C. M., (2006), *Mathematical modeling of biofilms*, IWA Publishing.

[39] Wanner O., and Gujer W., (1986), A Multispecies Biofilm Model, *Biotech. Bioeng.*, **28**(3), 314-328.

[40] Zhang T., Cogan N. G., and Wang Q., (2008), Phase Field Models for Biofilms, I. Theory and One-Dimensional Simulations, *SIAM J. Appl. Math.*, **69**, 641-669.

[41] Whitham G. B., (1974), *Linear and Nonlinear Waves*, John Wiley and Sons.

A ANALSYIS OF THE SEMI-DISCRETE (IN SPACE) MODEL

Semi-discretisation in space of (16)-(19) leads to cascades of twodimensional ordinary differential equations of the form

$$\frac{d}{dt}\begin{pmatrix} S_i \\ \lambda_i \end{pmatrix} = \begin{pmatrix} \dfrac{q}{(H-2\lambda_i)}(S_{i-1}-S_i) - \dfrac{X_\infty}{(H-2\lambda_i)}\, j(\lambda_i, S_i) + \dfrac{2S_i}{H-2\lambda_i}\dfrac{d\lambda_i}{ft}\, j(\lambda_i, S_i) + k\lambda_i - d(\lambda_i)\lambda_i \end{pmatrix}. \quad (28)$$

If $(s^*_{i-1}, \lambda^*_{i-1})$ is an equilibrium of the $(i-1)$th subsystem, then $(s^*_i, \lambda^*_i) = (s^*_{i-1}, 0)$ is a trivial equilibrium of (28) with Jacobian of the form

$$F'(S_{i-1}, 0) = \begin{pmatrix} -\dfrac{Q}{Lp} & * \\ 0 & \dfrac{\mu s^*_{i-1}}{\kappa + s^*_{i-1}} - k_d - d(0) \end{pmatrix}.$$

Thus, it has always one negative eigenvalue. The second eigenvalue is negative if $\frac{\mu s^*_{i-1}}{\kappa + s^*_{i-1}} - k_d - d(0) < 0$. Hence, the trivial equilibrium is stable if

$$s^*_{i-1} < \frac{\kappa(k_d + d(0))}{\mu - k_d - d(0)}, \quad (29)$$

and unstable if the reversed inequality holds. If the trivial equilibrium is unstable, a nontrivial equilibrium (s^*_i, λ^*_i) exists, for which

$$\frac{\mu s^*_{i-1}}{\kappa + s^*_{i-1}} - k_d - d(\lambda^*_i) = 0.$$

The Jacobian in such a point is

$$F'(s^*_i, \lambda^*_i) = \begin{pmatrix} -\dfrac{Q}{L(p-2\lambda_i)} - \dfrac{j_S(\lambda_i, S_i)}{H-2\lambda_i}\left(\dfrac{X_\infty}{Y} - 2S\right) & -\dfrac{2s^*_i\lambda^*_i}{p-2\lambda^*_i}\, d'(\lambda^*_i) \\ j_S(\lambda^*_i, s^*_i) & -d'(\lambda^*_i)\lambda^*_i \end{pmatrix}. \quad (30)$$

For realistic parameter, $\frac{X_\infty}{Y} \gg 2s^*_i$. Therefore, we have negative trace and positive determinant, i.e. such non-trivial equilibria are stable.

Overall, the equilibria of the cascade of ODEs (28) are chains of equilibria of the subsystems. An equilibrium of the semi-discrete system is stable if it is composed of stable equilibria of the subsystems, otherwise unstable.